Electronic Supplementary Information (ESI)

Controllable chiral memory in an anion tetrahedral cage

Wenyao Zhang,[a,c,#] Jie Zhao,[a,#] Dong Yang,[a,*] Boyang Li,[a] Yang Feng,[a] Yue Wang,[a] Xiaoyan Zheng,[b] Xiao-Juan Yang[b] and Biao Wu[a,b,*]

[a]Key Laboratory of Synthetic and Natural Functional Molecule of the Ministry of Education, College of Chemistry and Materials Science, Northwest University, Xi'an 710069, China. E-mail: yangdong@nwu.edu.cn. [b]Key Laboratory of Medicinal Molecule Science and Pharmaceutics Engineering, Ministry of Industry and Information Technology, School of Chemistry and Chemical Engineering, Beijing Institute of Technology, Beijing 100081, China. E-mail: wubiao@bit.edu.cn. [c]Key Laboratory of Magnetic Molecules and Magnetic Information Materials of Ministry of Education, School of Chemistry and Materials Science, Shanxi Normal University, TaiYuan 030031, China.

Table of Contents

S1. General considerations 2
S2. ^{1}H and 2D NMR spectra 2
S3. Circular dichroism (CD) characterization of chiral induction 9
S4. Calculations of chiral induction and memory 11
S5. Binding constant 15
S6. High-resolution ESI-MS spectra 18
S7. Energy calculations 20
S8. X-ray crystallography 21
S9. References 24

S1. General considerations

The *o*-nitrophenylisocyanate and *p*-nitrophenylisocyanate were purchased from Alfa Aesar. All solvents and other reagents were of reagent grade quality. ^{1}H NMR spectra were obtained by using Bruker Avance III-400 MHz and JNM-ECZ400S spectrometers unless noted otherwise. ^{1}H chemical shifts were based on the residual solvent peaks as the internal standard (1.94 ppm for CD_3CN). All the ESI-MS measurements were carried out using a Bruker Daltonics micrOTOF-Q II mass spectrometer. Circular Dichroism (CD) spectra were recorded on a J-1500 spectropolarimeter (Jasco, Japan), using a 1 mm quartz cuvette. UV/vis spectra were done on Agilent Cray-100 spectrometer. Cage **1**[1] and trifluoromethanesulfonate salts of enantiopure R/S-α-methylcholine ($G^{1S/R}$), and R/S-β-methylcholine ($G^{2S/R}$)[2] were synthesized according to our previous work.

S2. ^{1}H and 2D NMR spectra

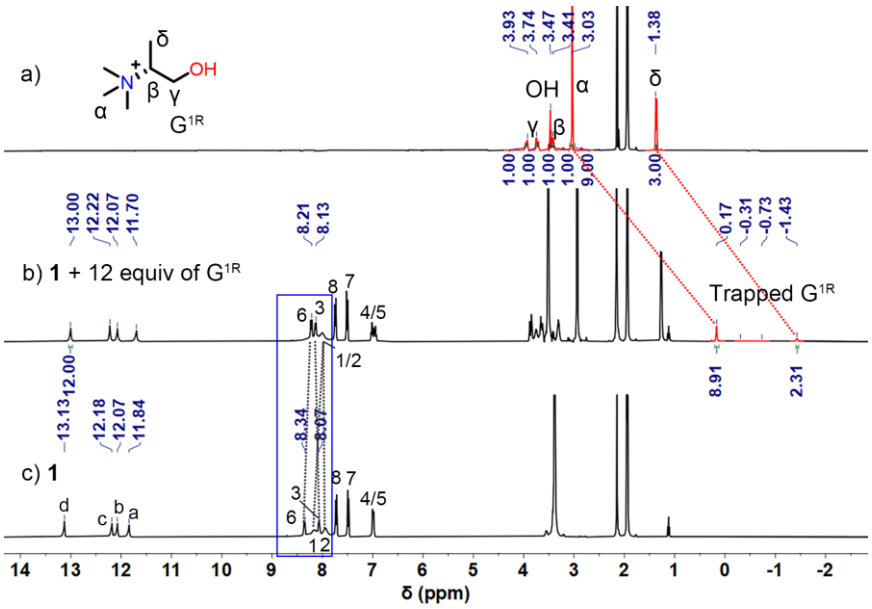

Fig. S1 ^{1}H NMR spectra (400 MHz, CD_3CN, 298 K, 0.5 mM) of a) G^{1R}, b) **1** with 12 equiv of G^{1R}, and c) **1** (changes of the chemical shifts of H1, H2, H3 and H6 are indicated by blue rectangle, and the signals for trapped G^{1R} are shown in red).

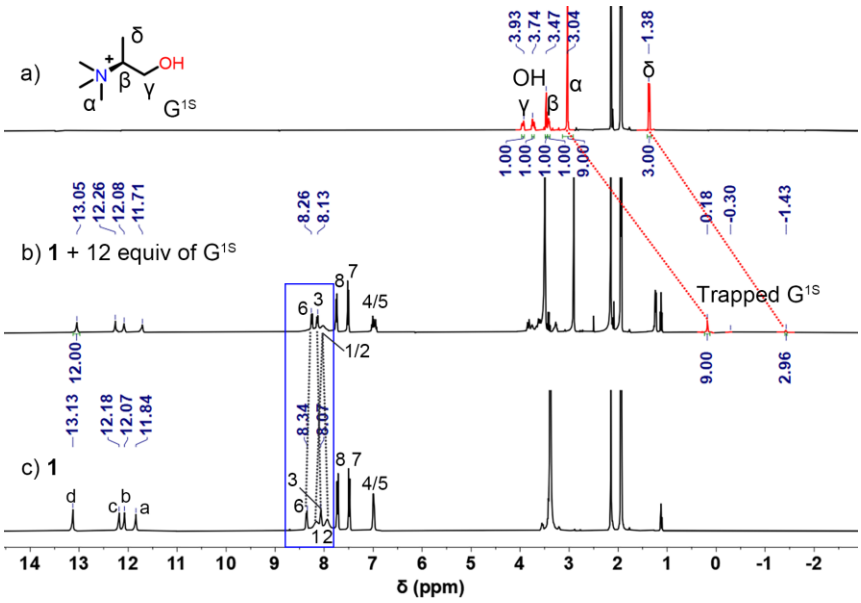

Fig. S2 ^{1}H NMR spectra (400 MHz, CD_3CN, 298 K, 0.5 mM) of a) G^{1S}, b) **1** with 12 equiv of G^{1S}, and c) **1** (changes of the chemical shifts of H1, H2, H3 and H6 are indicated by blue rectangle, the signals for trapped G^{1S} are shown in red).

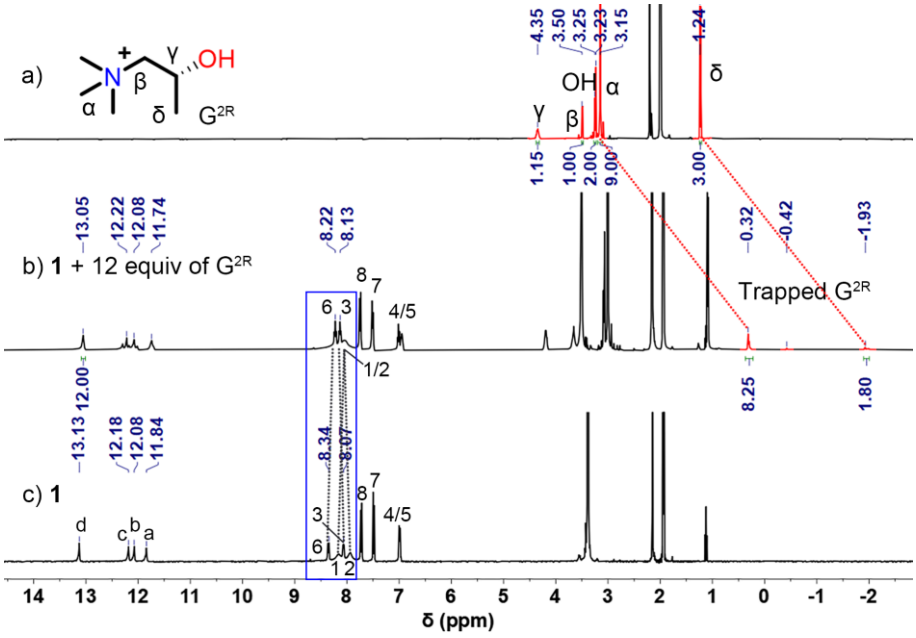

Fig. S3 ^{1}H NMR spectra (400 MHz, CD_3CN, 298 K, 0.5 mM) of a) G^{2R}, b) **1** with 12 equiv of G^{2R}, and c) **1** (changes of the chemical shifts of H1, H2, H3 and H6 are indicated by blue rectangle, the signals for trapped G^{2R} are shown in red).

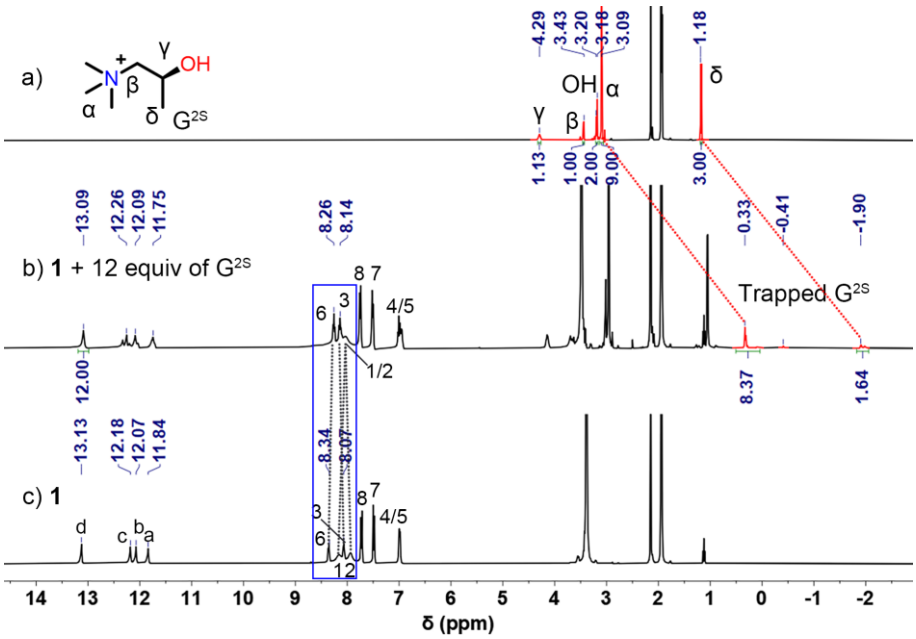

Fig. S4 ^{1}H NMR spectra (400 MHz, CD_3CN, 298 K, 0.5 mM) of a) G^{2S}, b) **1** with 12 equiv of G^{2S}, and c) **1** (changes of the chemical shifts of H1, H2, H3 and H6 are indicated by blue rectangle, the signals for trapped G^{2S} are shown in red).

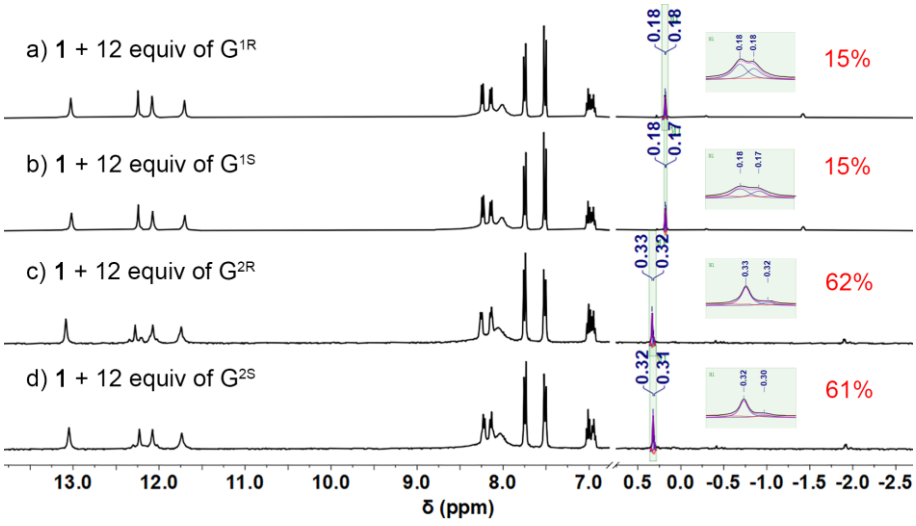

Fig. S5 ^{1}H NMR spectra (400 MHz, CD_3CN, 298 K, 0.5 mM) of a) **1** with 12 equiv of G^{1R}, b) **1** with 12 equiv of G^{1S}, c) **1** with 12 equiv of G^{2R} and d) **1** with 12 equiv of G^{2S}, the *de* values were calculated from the integration ratio of the signals of trapped guest.

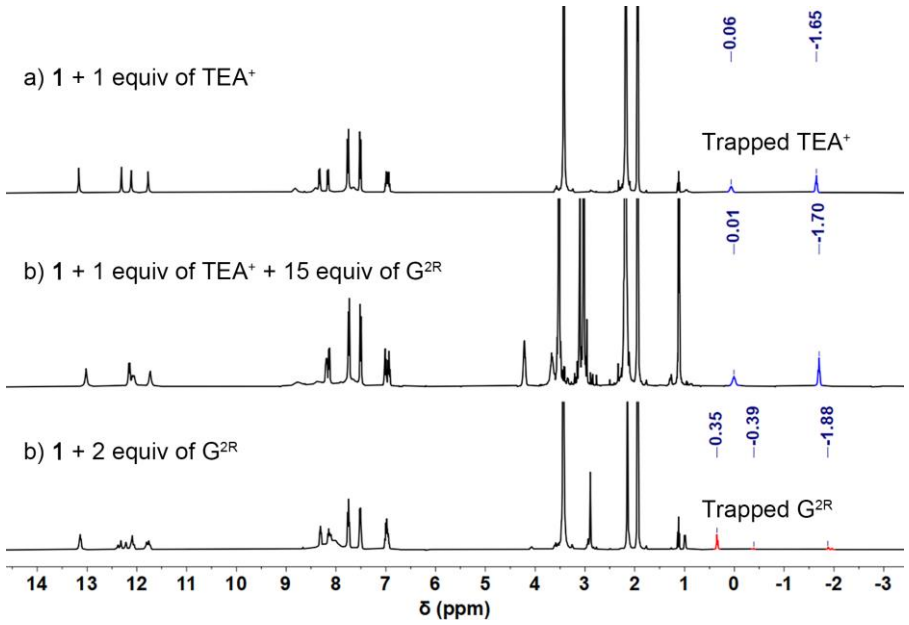

Fig. S6 ^{1}H NMR spectra (400 MHz, CD_3CN, 298 K, 500 μM) of a) **1** with 1 equiv of TEA^+, b) **1** with 1 equiv of TEA^+ and 15 equiv of G^{2R}, c) **1** with 2 equiv of G^{2R} (the signals for trapped TEA^+ are shown in blue, G^{2R} in red).

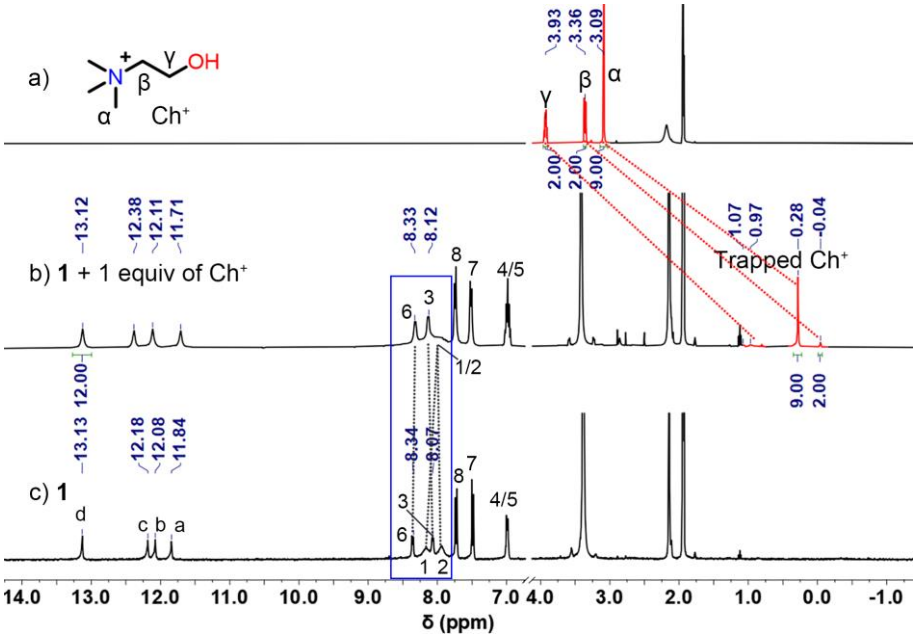

Fig. S7 ^{1}H NMR spectra (400 MHz, CD_3CN, 298 K, 0.5 mM) of a) Ch^+, b) **1** with 1 equiv of Ch^+, and c) **1** (changes of the chemical shifts of H1, H2, H3 and H6 are indicated by blue rectangle, the signals for trapped Ch^+ are shown in red).

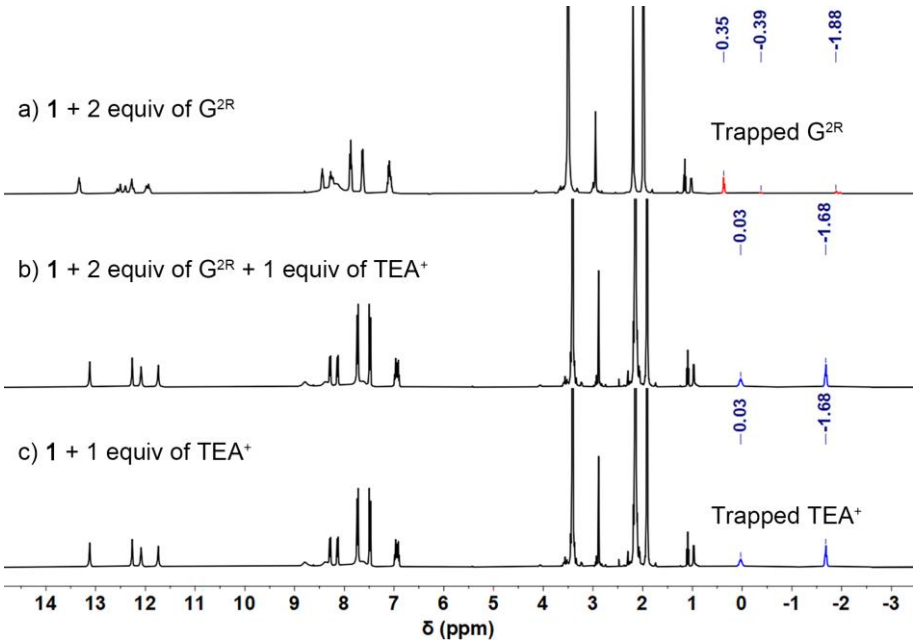

Fig. S8 ^{1}H NMR spectra (400 MHz, CD_3CN, 298 K, 0.5 mM) of a) **1** with 2 equiv of G^{2R}, b) **1** with 2 equiv of G^{2R} and 1 equiv of TEA^+, c) **1** with 1 equiv of TEA^+ (the signals for trapped TEA^+ are shown in blue, and those for G^{2R} are in red).

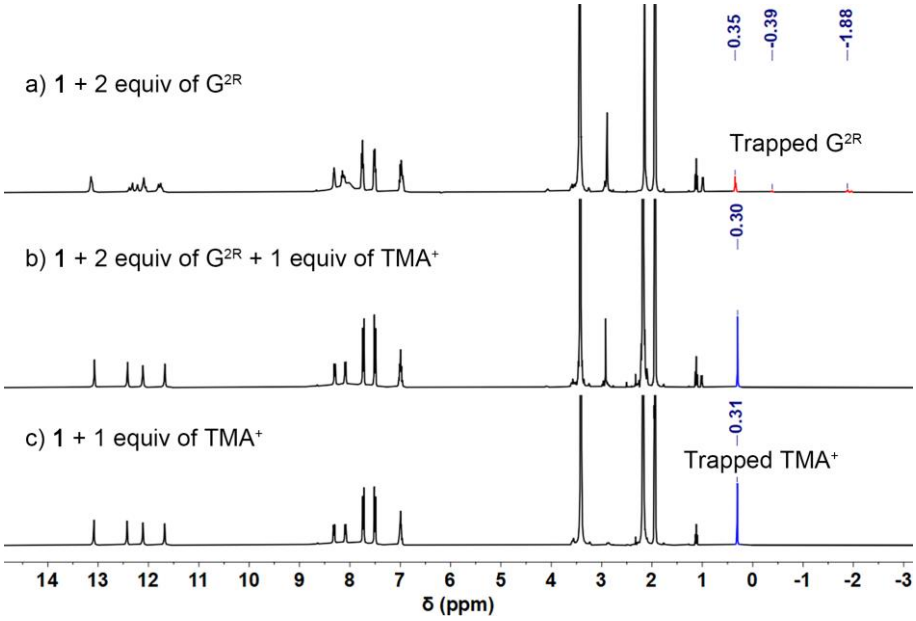

Fig. S9 ^{1}H NMR spectra (400 MHz, CD_3CN, 298 K, 0.5 mM) of a) **1** with 2 equiv of G^{2R}, b) **1** with 2 equiv of G^{2R} and 1 equiv of TMA^+, c) **1** with 1 equiv of TMA^+ (the signals for trapped TMA^+ are shown in blue, and those for G^{2R} are in red).

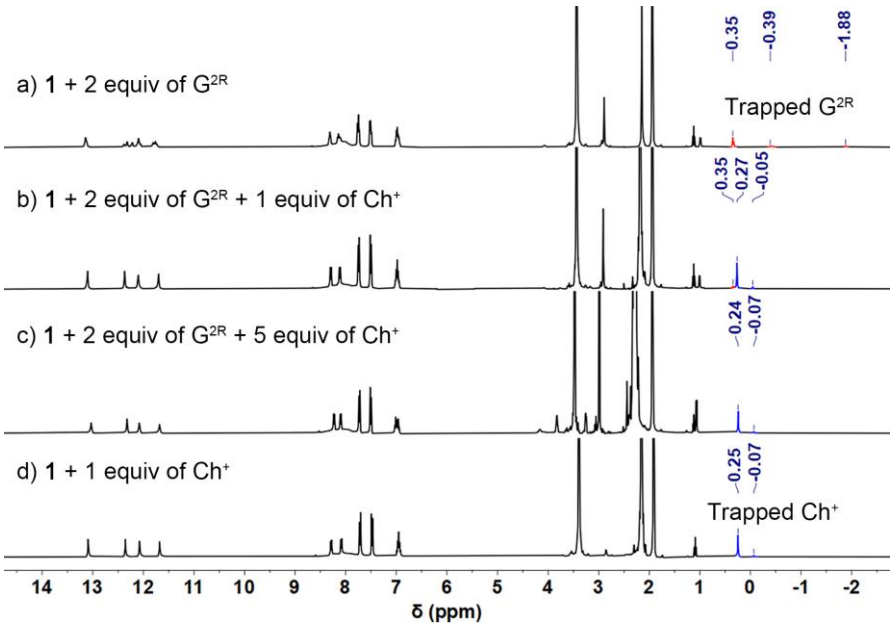

Fig. S10 ^{1}H NMR spectra (400 MHz, CD_3CN, 298 K, 0.5 mM) of a) **1** with 2 equiv of G^{2R}, b) **1** with 2 equiv of G^{2R} and 1 equiv of Ch^+ (around 90 % of G^{2R} were replaced by 1 equiv of Ch^+), c) **1** with 2 equiv of G^{2R} and 5 equiv of Ch^+, d) **1** with 1 equiv of Ch^+ (the signals for trapped Ch^+ are shown in blue).

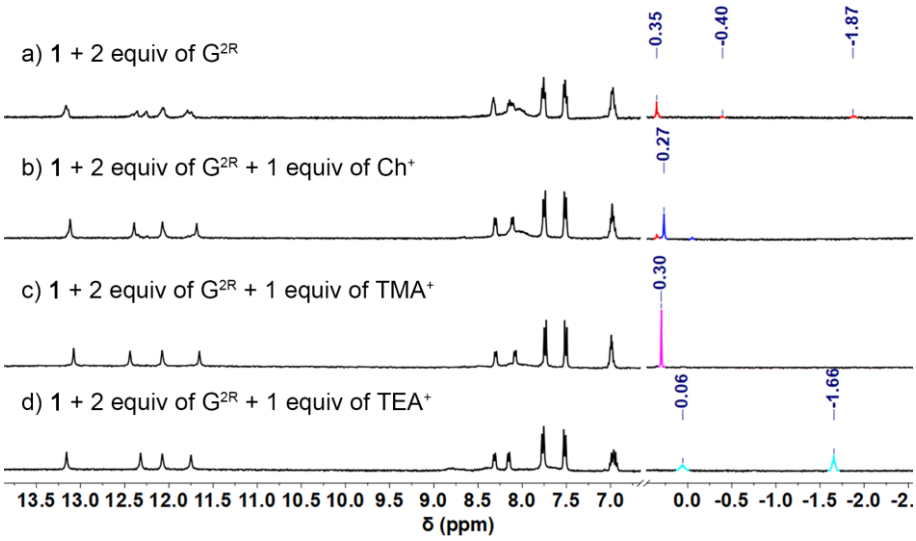

Fig. S11 ^{1}H NMR spectra (400 MHz, CD_3CN, 298 K, 50 μM) of a) **1** with 2 equiv of G^{2R}, b) **1** with 2 equiv of G^{2R} and 1 equiv of Ch^+, c) **1** with 2 equiv of G^{2R} and 1 equiv of TMA^+, d) **1** with 2 equiv of G^{2R} and 1 equiv of TEA^+.

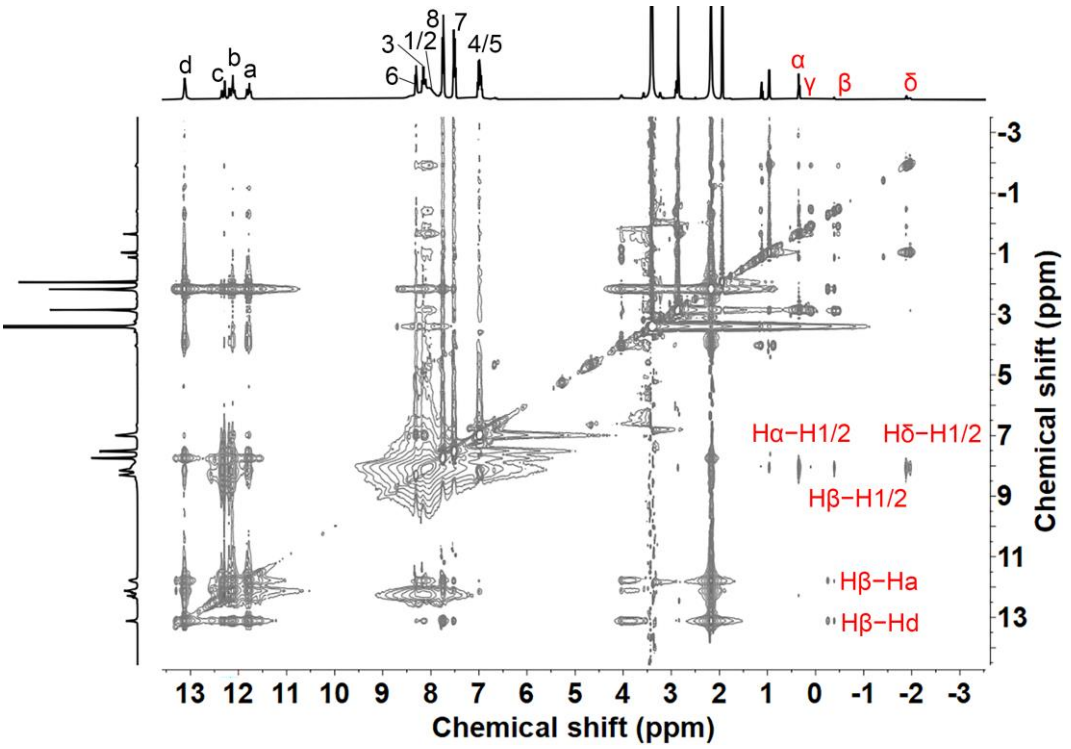

Fig. S12 ^{1}H-^{1}H NOESY spectrum (400 MHz, CD_3CN, 298 K) of **1** with 2 equiv of G^{2R}.

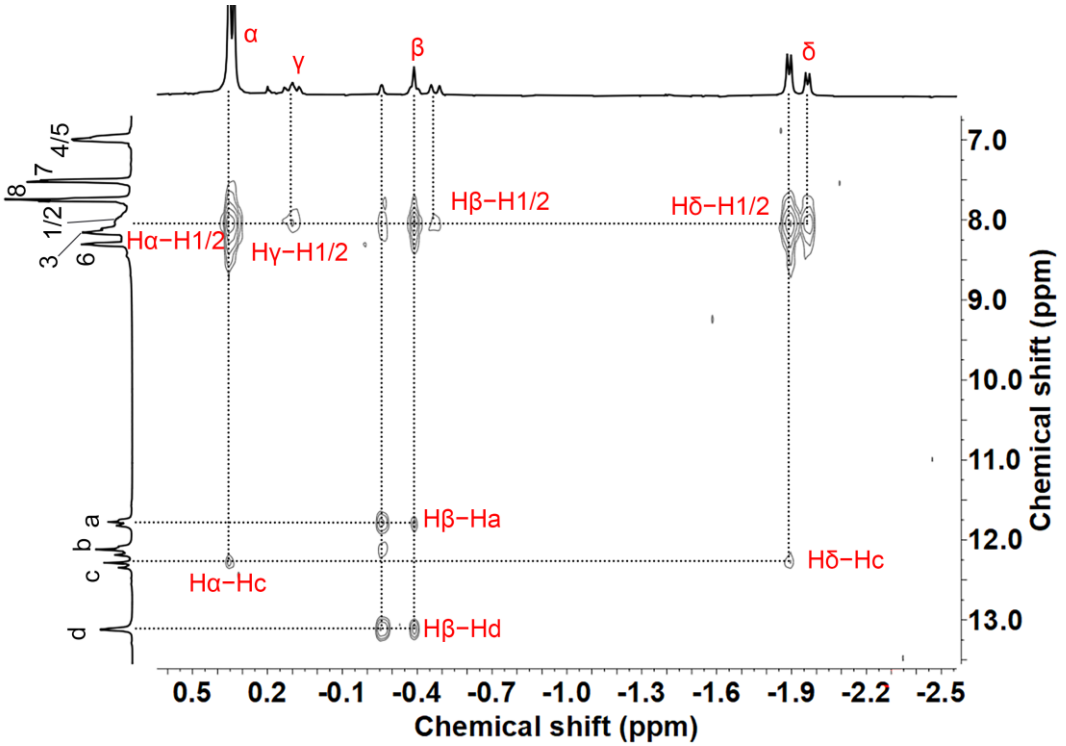

Fig. S13 Partial ^{1}H-^{1}H NOESY spectrum (400 MHz, CD_3CN, 298 K) of **1** with 2 equiv of G^{2R}.

S3. Circular dichroism (CD) characterization of chiral induction

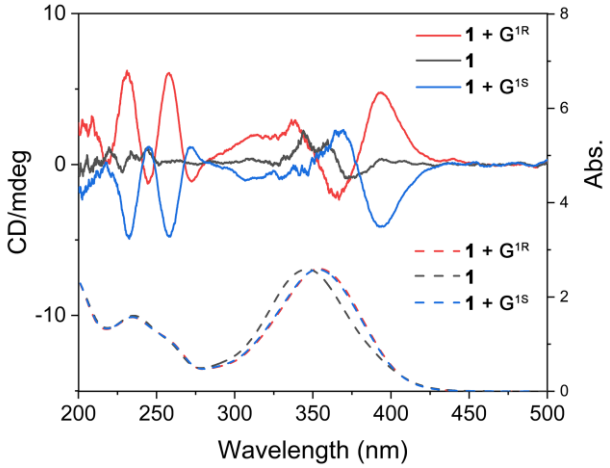

Fig. S14 CD and UV-vis spectra of **1** (50 μM) before and after addition of 12 equiv of enantiomers of $G^{1R/1S}$.

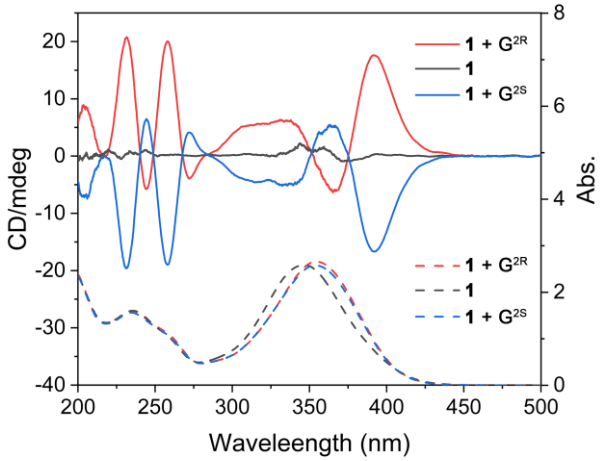

Fig. S15 CD and UV-vis spectra of **1** (50 μM) before and after addition of 12 equiv of enantiomers of $G^{2R/2S}$.

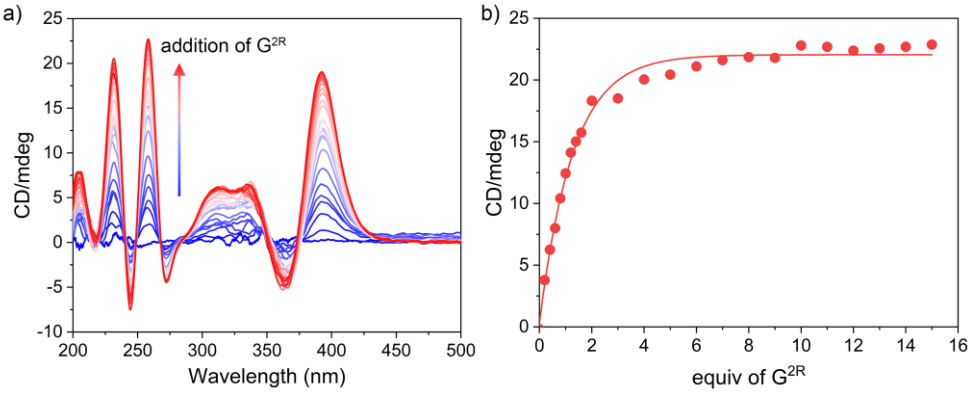

Fig. S16 a) CD spectra of **1** (50 μM, CH_3CN) with addition of different equiv of G^{2R} (from 0 to 15 equiv), b) CD intensity of **1** (50 μM, CH_3CN) with addition of different equiv of G^{2R} at λ = 258 nm.

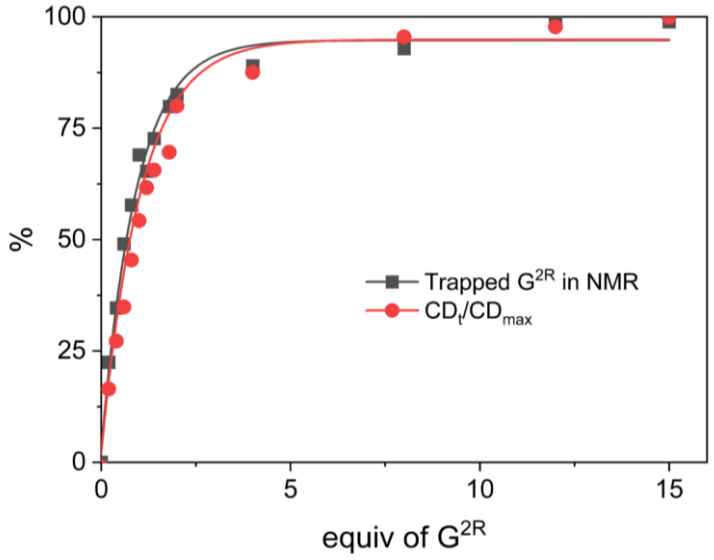

Fig. S17 Plots of the integral areas of trapped G^{2R} in NMR (0.5 mM, CD_3CN) and CD intensity at λ = 258 nm (50 μM, CH_3CN) versus the equiv of G^{2R}.

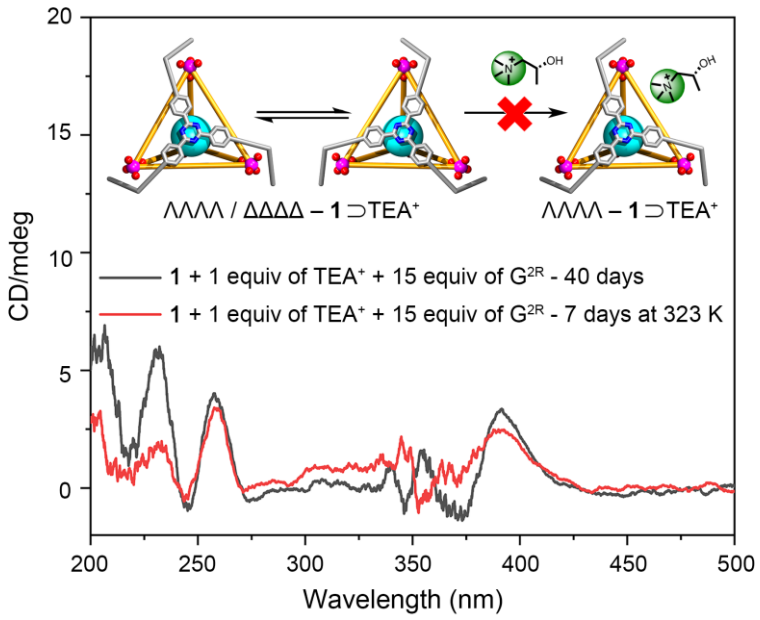

Fig. S18 CD spectra of cage **1**⊃TEA^+ (50 μM) before and after addition of 15 equiv G^{2R} after equilibrated for 40 days or heated at 323 K for 7 days.

S4. Calculations of chiral induction and memory

The calculations of rate constants, which were dependent on the first-order kinetic model[3-5], are based on the equations:

$$(\Delta\Delta\Delta\Delta)\text{-}\mathbf{1} \xrightarrow{k_{obs}} (\Lambda\Lambda\Lambda\Lambda)\text{-}\mathbf{1} \qquad (1)$$

$$(\Delta\Delta\Delta\Delta)\text{-}\mathbf{1} \underset{k_{-1}}{\overset{k_1}{\rightleftharpoons}} (\Lambda\Lambda\Lambda\Lambda)\text{-}\mathbf{1}$$

$$\ln (CD_t/CD_0) = -2k_1 t \qquad (2)$$

the k_1 (s^{-1}) is the rate constant for racemization, and the half-life time ($t_{1/2}$) was obtained from equation (3):

$$t_{1/2} = \ln 2/2k_1 = 0.693/2k_1 \qquad (3)$$

The activation enthalpy ($\Delta H^{\ddagger}$), entropy ($\Delta S^{\ddagger}$) and Gibbs free energy ($\Delta G^{\ddagger}$) were obtained from the Eyring equation:

$$\ln(k_1/T) = \Delta S^{\ddagger}/R - \ln(h/k_B) - \Delta H^{\ddagger}/(RT) \qquad (4)$$

in which h is the Planck's constant, k_B is the Boltzmann constant, R (8.314 J K^{-1} mol^{-1}) is the gas constant, T (K) is the absolute temperature.

The activation Gibbs free energy ($\Delta G^{\ddagger}$) were obtained from $\Delta H^{\ddagger}$ and $\Delta S^{\ddagger}$.

$$\Delta G^{\ddagger} = \Delta H^{\ddagger} - T\Delta S^{\ddagger}$$

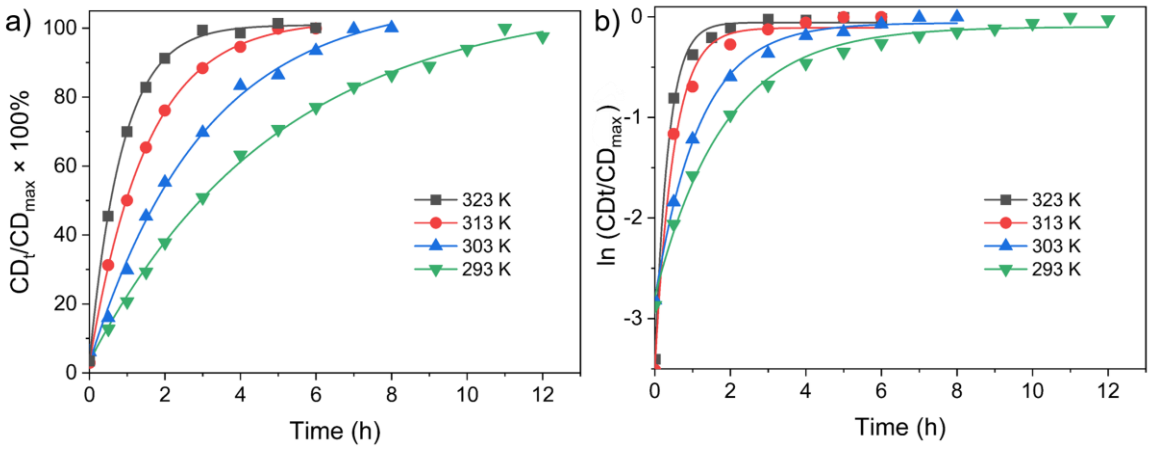

Fig. S19 a) CD signal changes and b) plot of ln (CD_t/CD_{max}) of **1** with 12 equiv of G^{2R} at 258 nm against time at different temperatures.

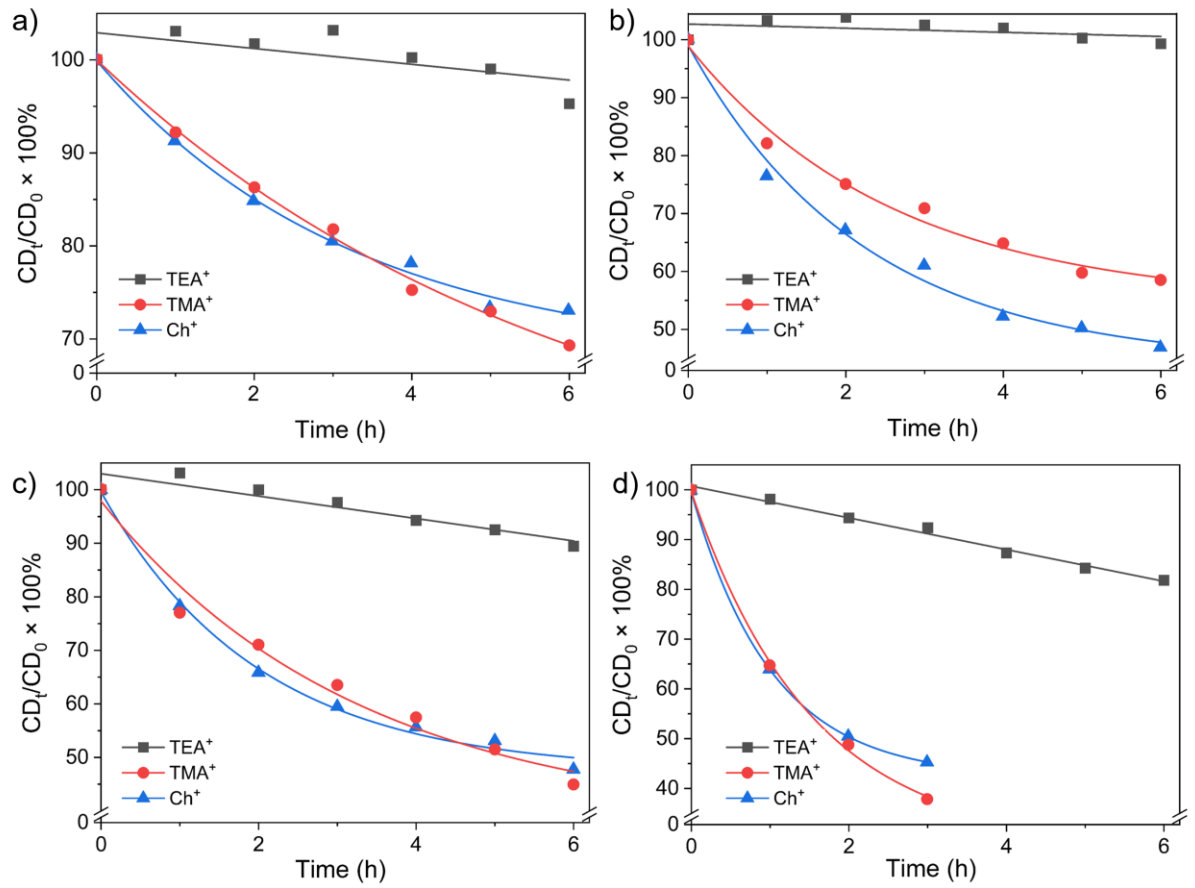

Fig. S20 CD signal changes of **1** with 2 equiv of G^{2R} at 258 nm against time by the addition of 1 equiv of TEA^+, TMA^+ and Ch^+ at a) 283 K, b) 293 K, c) 303 K, and d) 313 K.

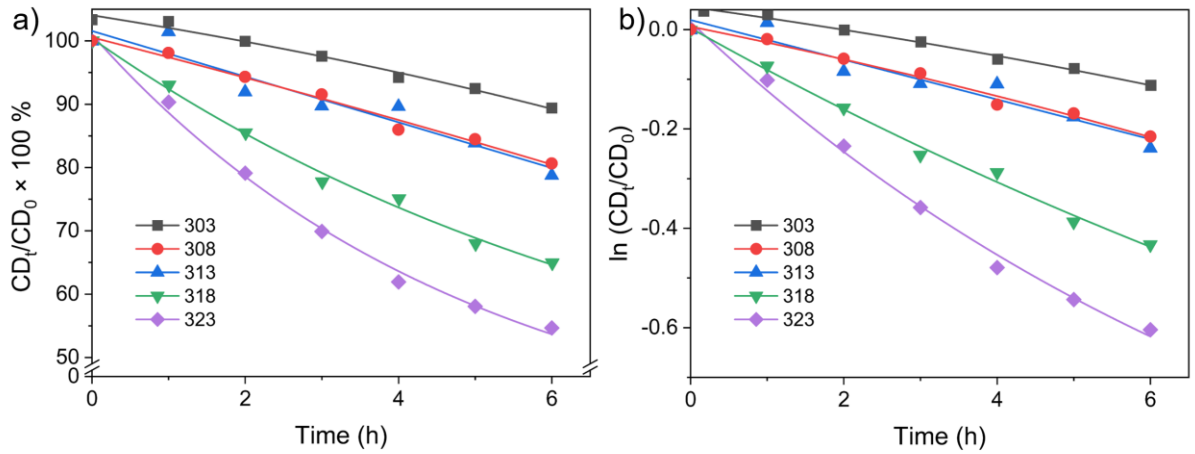

Fig. S21 a) CD signal changes and b) plot of ln (CD_t/CD_0) of **1** with 2 equiv of G^{2R} at 258 nm against time by the addition of 1 equiv of TEA^+ at different temperatures.

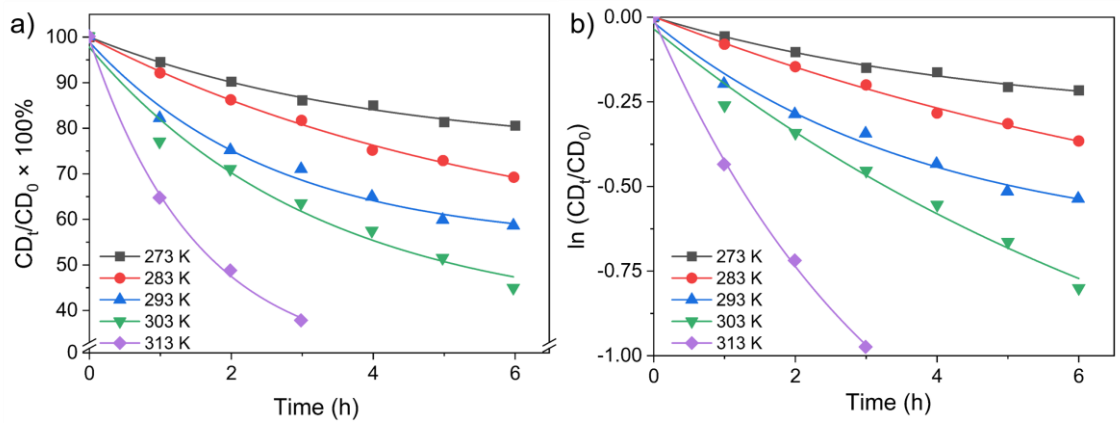

Fig. S22 a) CD signal changes and b) plot of ln (CD_t/CD_0) of **1** with 2 equiv of G^{2R} at 258 nm against time by the addition of 1 equiv of TMA^+ at different temperatures.

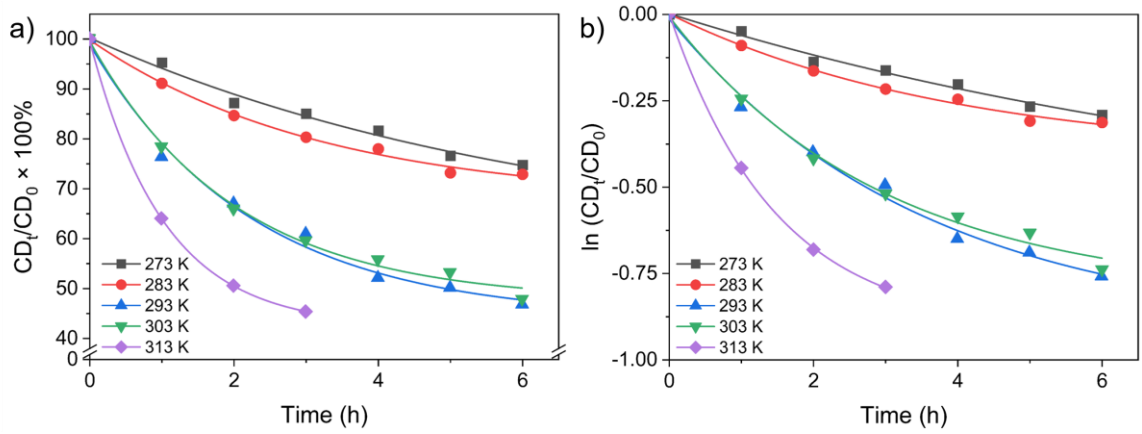

Fig. S23 a) CD signal changes and b) plot of ln (CD_t/CD_0) of **1** with 2 equiv of G^{2R} at 258 nm against time by the addition of 1 equiv of Ch^+ at different temperatures.

Table S1 Rate constant k_1 of chiral induction by 12 equiv of G^{2R} at different temperatures.

k_1 (s^{-1})	293 K	303 K	313 K	323 K
	$(1.80 \pm 0.13) \times 10^{-4}$	$(2.66 \pm 0.14) \times 10^{-4}$	$(3.44 \pm 0.15) \times 10^{-4}$	$(4.00 \pm 0.11) \times 10^{-4}$

Table S2 Rate constant k_1 of TEA^+ at different temperatures.

k_1 (s^{-1})	303 K	308 K	313 K	318 K	323 K
TEA^+	$(3.66 \pm 0.16) \times 10^{-6}$	$(5.15 \pm 0.28) \times 10^{-6}$	$(6.54 \pm 0.20) \times 10^{-6}$	$(1.04 \pm 0.03) \times 10^{-5}$	$(1.58 \pm 0.07) \times 10^{-5}$

Table S3 Rate constant k_1 of TMA^+ at different temperatures.

k_1 (s^{-1})	273 K	283 K	293 K	313 K
TMA^+	$(3.79 \pm 0.25) \times 10^{-6}$	$(8.48 \pm 0.41) \times 10^{-6}$	$(1.33 \pm 0.14) \times 10^{-5}$	$(4.44 \pm 0.20) \times 10^{-5}$

Table S4 Rate constant k_1 of Ch^+ at different temperatures.

k_1 (s^{-1})	273 K	283 K	293 K	313 K
Ch^+	$(6.81 \pm 0.44) \times 10^{-6}$	$(2.00 \pm 0.11) \times 10^{-5}$	$(2.49 \pm 0.17) \times 10^{-5}$	$(4.06 \pm 0.29) \times 10^{-5}$

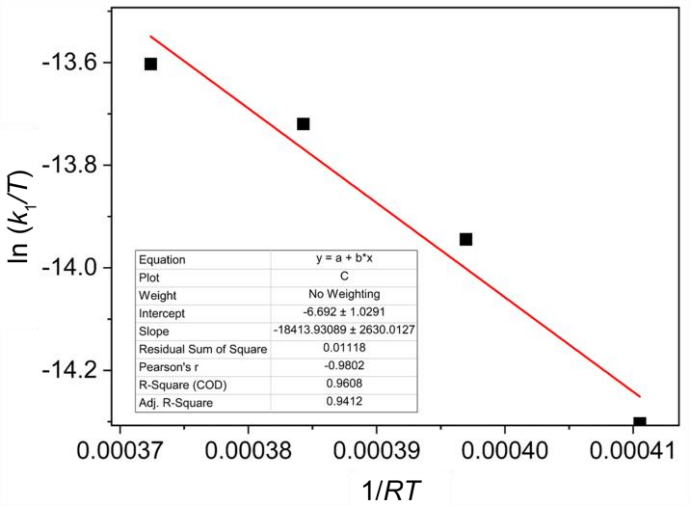

Fig. S24 Erying plots of ln(k_1/T) versus 1/RT for the determination of the activation enthalpy ($\Delta H^{\ddagger}$) and entropy ($\Delta S^{\ddagger}$) for chiral induction of 12 equiv of G^{2R}.

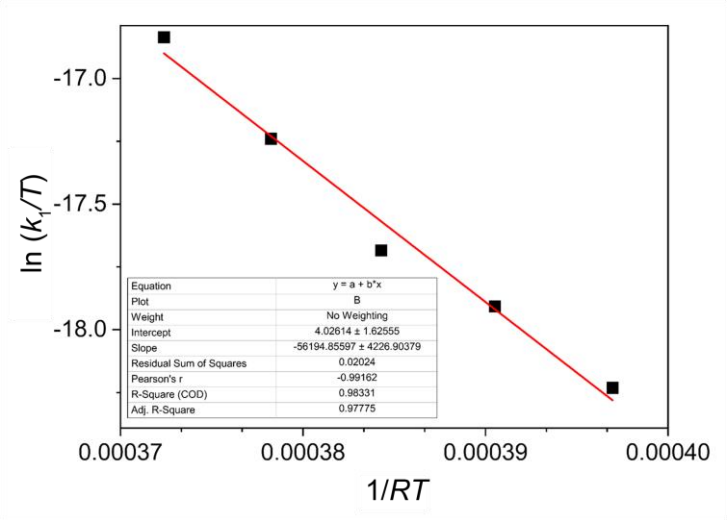

Fig. S25 Erying plots of ln(k_1/T) versus 1/RT for the determination of the activation enthalpy ($\Delta H^{\ddagger}$) and entropy ($\Delta S^{\ddagger}$) for racemization of **1**⊃TEA^+.

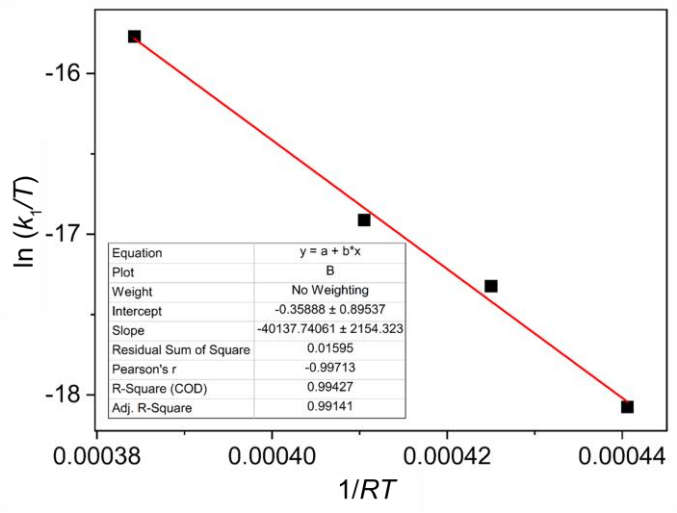

Fig. S26 Erying plots of ln(k_1/T) versus 1/RT for the determination of the activation enthalpy ($\Delta H^{\ddagger}$) and entropy ($\Delta S^{\ddagger}$) for racemization of **1**⊃TMA^+.

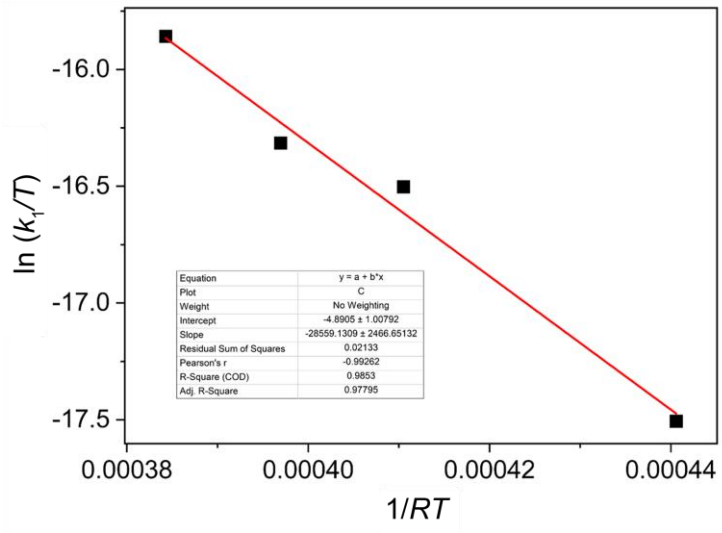

Fig. S27 Erying plots of ln(k_1/T) versus 1/RT for the determination of the activation enthalpy ($\Delta H^{\ddagger}$) and entropy ($\Delta S^{\ddagger}$) for racemization of **1**⊃Ch^+.

S5. Binding constant

The binding constants were determined by ^{1}H NMR titrations[6] (in 1 : 1 model). All ^{1}H NMR titrations were performed at room temperature. In the titrations the guest was added to a 500 μL of cage with 1,3,5-trimethoxybenzene (0.5 mM) as internal standard in CD_3CN.

The equilibrium between a host *H* and a guest *G* that can form host-guest complex *HG*:

$$\mathbf{H + G \rightleftharpoons HG}$$

Binding constant *K* for this equilibrium is defined as:

$$K = \frac{[\mathrm{HG}]}{[\mathrm{H}][\mathrm{G}]}$$

Using origin to fit the binding data,

Y=Y0+DY*((Ka*(P+x)+1)–SQRT(((Ka*(P+x)+1)^2)–4*Ka*Ka*P*x))/(2*Ka*P)

Y Measured Integral Area

Y0 Integral Area of empty host solution

DY Maximal change in Integral Area: the difference in Integral Area of a fully occupied host and an empty host

*K*a Binding constant

P Total host concentration

x Total guest concentration

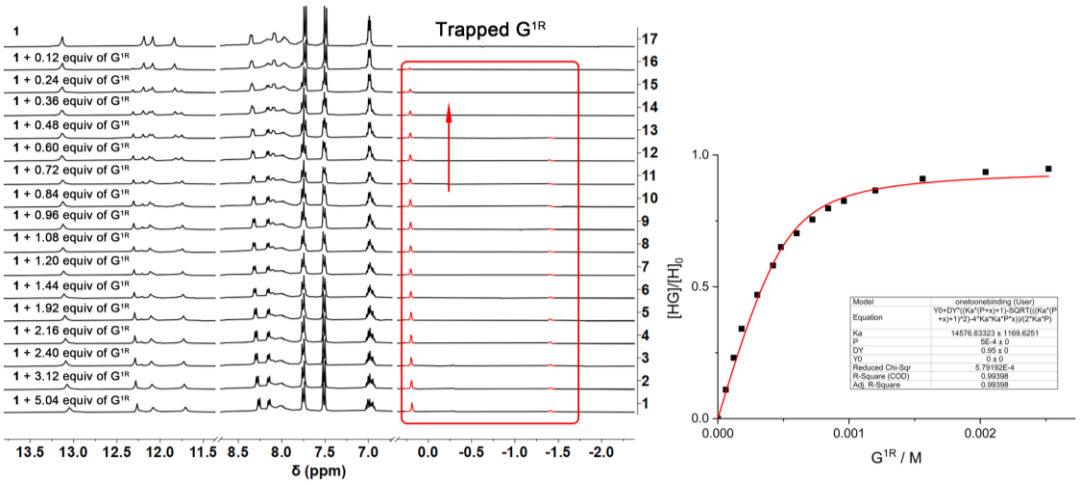

Fig. S28 Partial ^{1}H NMR spectra (400 MHz, 298 K, CD_3CN) of **1** (0.5 mM, both **1** and guest were corrected by 1,3,5-trimethoxybenzene) upon addition of 0-5.04 equiv of G^{1R} (the signals for **1**⊃G^{1R} are shown in red, left), and data fitting for the titration of the slow exchange G^{1R} guest into a solution of **1** (right). A binding constant of $(1.46 \pm 0.12) \times 10^4$ M^{-1} was calculated for **1**⊃G^{1R}.

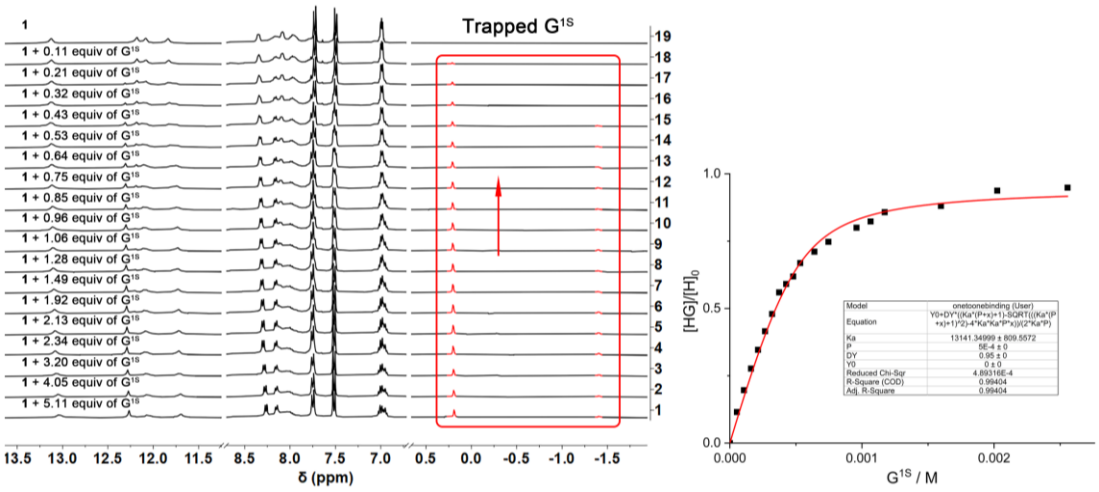

Fig. S29 Partial ^{1}H NMR spectra (400 MHz, 298 K, CD_3CN) of **1** (0.5 mM, both **1** and guest were corrected by 1,3,5-trimethoxybenzene) upon addition of 0-5.11 equiv of G^{1S} (the signals for **1**⊃G^{1S} are shown in red, left), and data fitting for the titration of the slow exchange G^{1S} guest into a solution of **1** (right). A binding constant of $(1.31 \pm 0.08) \times 10^4$ M^{-1} was calculated for **1**⊃G^{1S}.

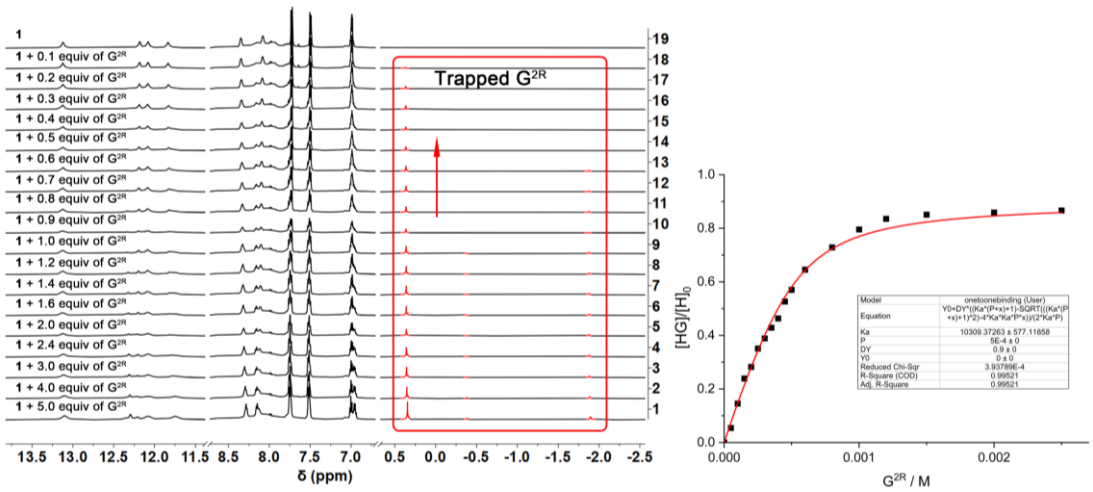

Fig. S30 Partial ^{1}H NMR spectra (400 MHz, 298 K, CD_3CN) of **1** (0.5 mM, both **1** and guest were corrected by 1,3,5-trimethoxybenzene) upon addition of 0-5.0 equiv of G^{2R} (the signals for **1**⊃G^{2R} are shown in red, left), and data fitting for the titration of the slow exchange G^{2R} guest into a solution of **1** (right). A binding constant of $(1.03 \pm 0.06) \times 10^4$ M^{-1} was calculated for **1**⊃G^{2R}.

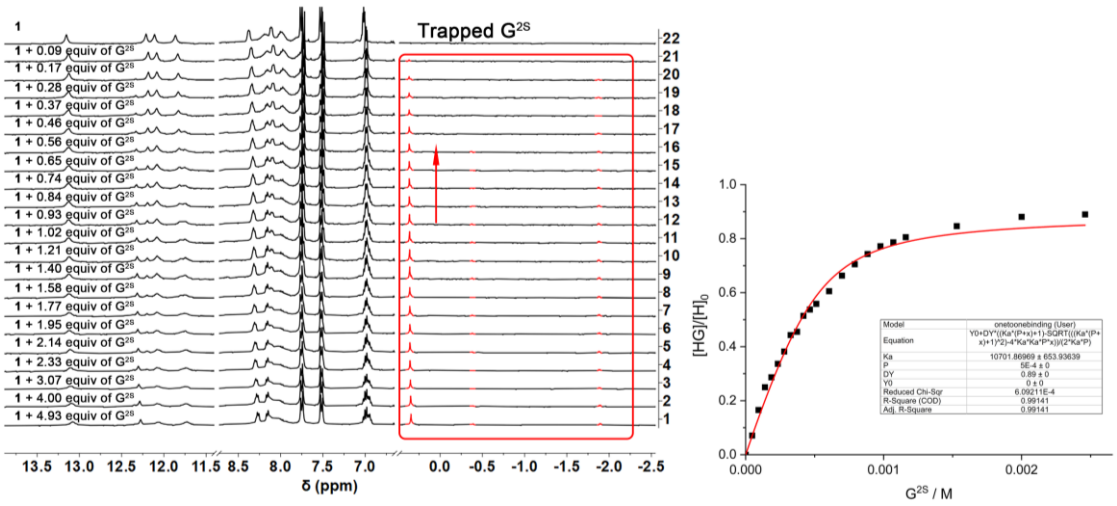

Fig. S31 Partial ^{1}H NMR spectra (400 MHz, 298 K, CD_3CN) of **1** (0.5 mM, both **1** and guest were corrected by 1,3,5-trimethoxybenzene) upon addition of 0-4.93 equiv of G^{2S} (the signals for **1**⊃G^{2S} are shown in red, left), and data fitting for the titration of the slow exchange G^{2S} guest into a solution of **1** (right). A binding constant of $(1.07 \pm 0.06) \times 10^4$ M^{-1} was calculated for **1**⊃G^{2S}.

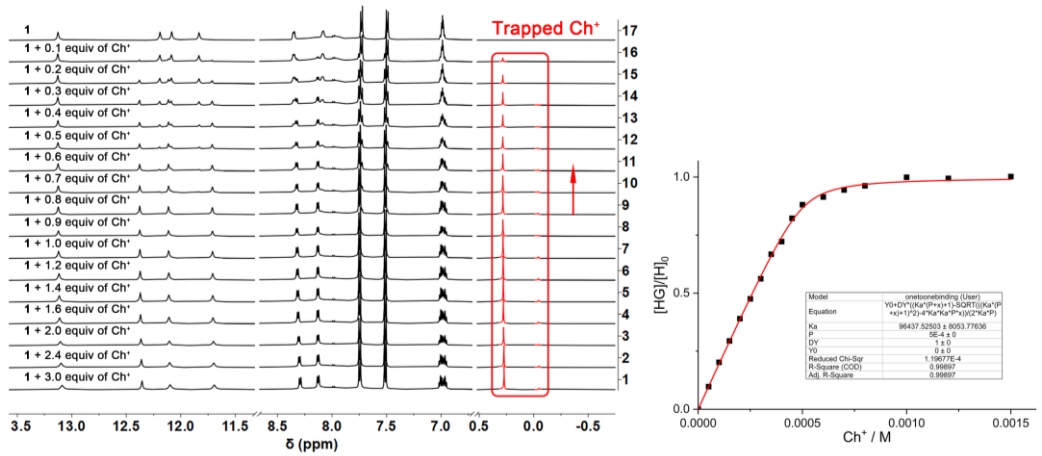

Fig. S32 Partial ^{1}H NMR spectra (400 MHz, 298 K, CD_3CN) of **1** (0.5 mM, both **1** and guest were corrected by 1,3,5-trimethoxybenzene) upon addition of 0-3.0 equiv of Ch^+ (the signals for **1**⊃Ch^+ are shown in red, left), and data fitting for the titration of the slow exchange Ch^+ guest into a solution of **1** (right). A binding constant of (9.64 ± 0.80) × 10^4 M^{-1} was calculated for **1**⊃Ch^+.

S6. High-resolution ESI-MS spectra

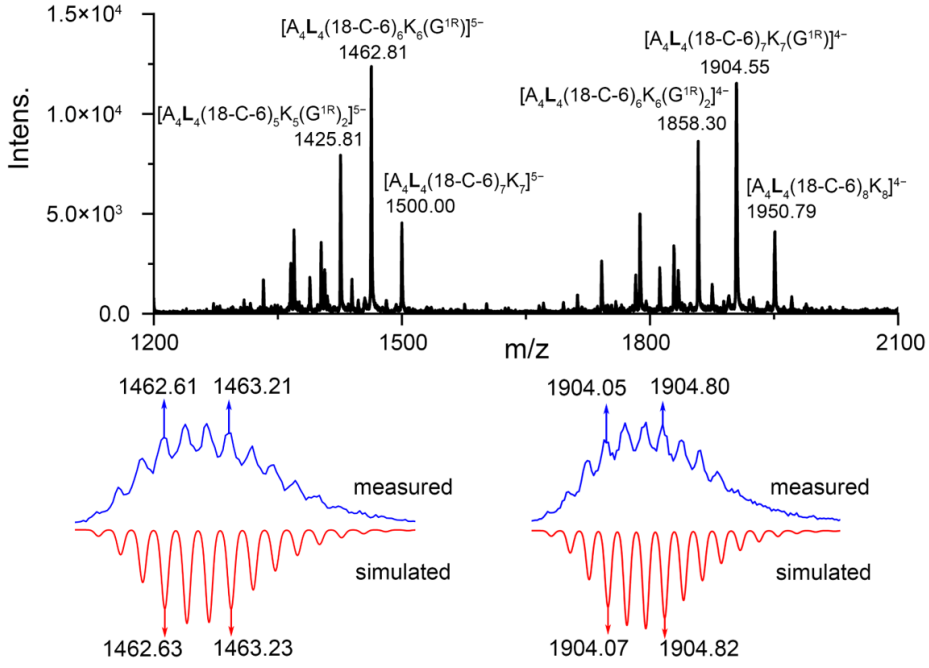

Fig. S33 High-resolution ESI-mass spectrum of **1**⊃G^{1R}.

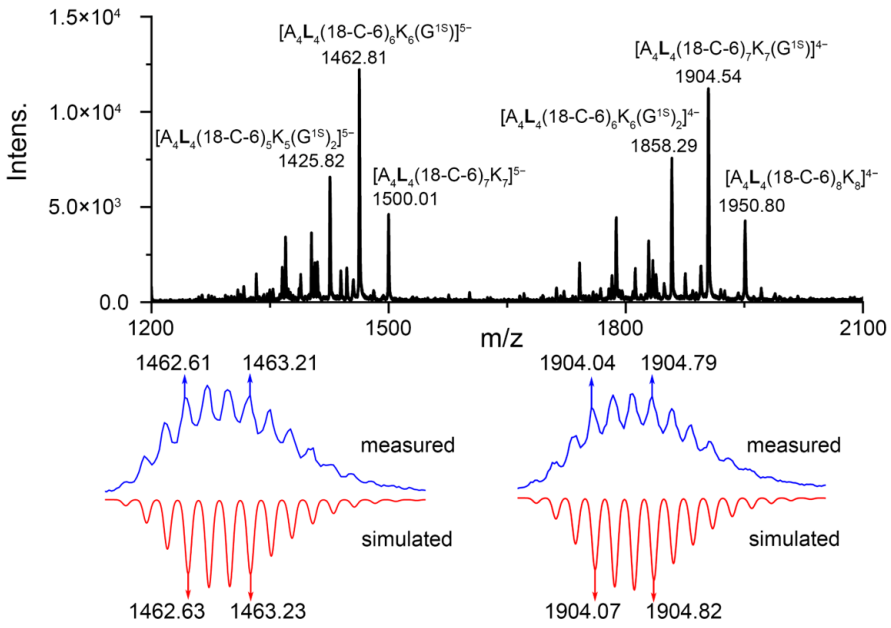

Fig. S34 High-resolution ESI-mass spectrum of **1**⊃G^{1S}.

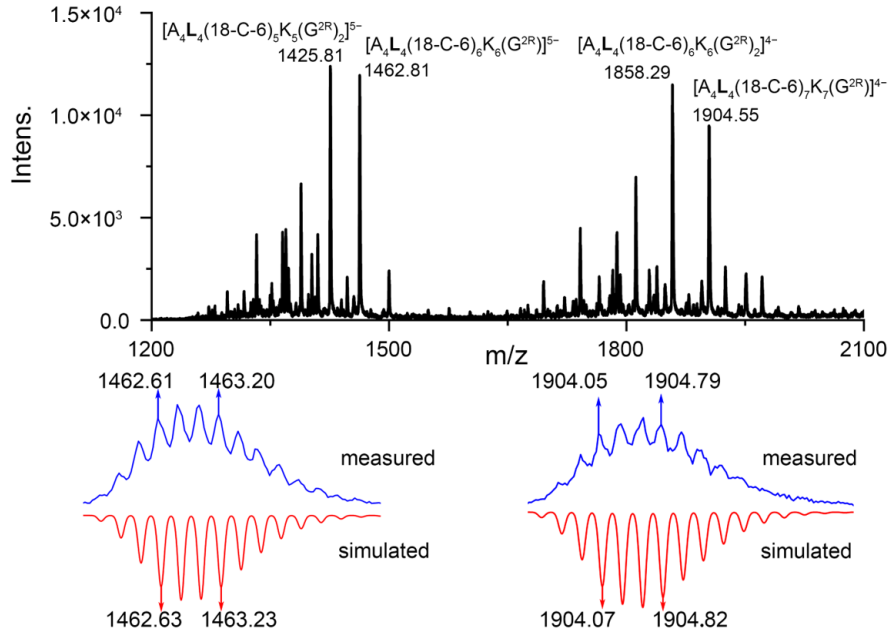

Fig. S35 High-resolution ESI-mass spectrum of **1**⊃G^{2R}.

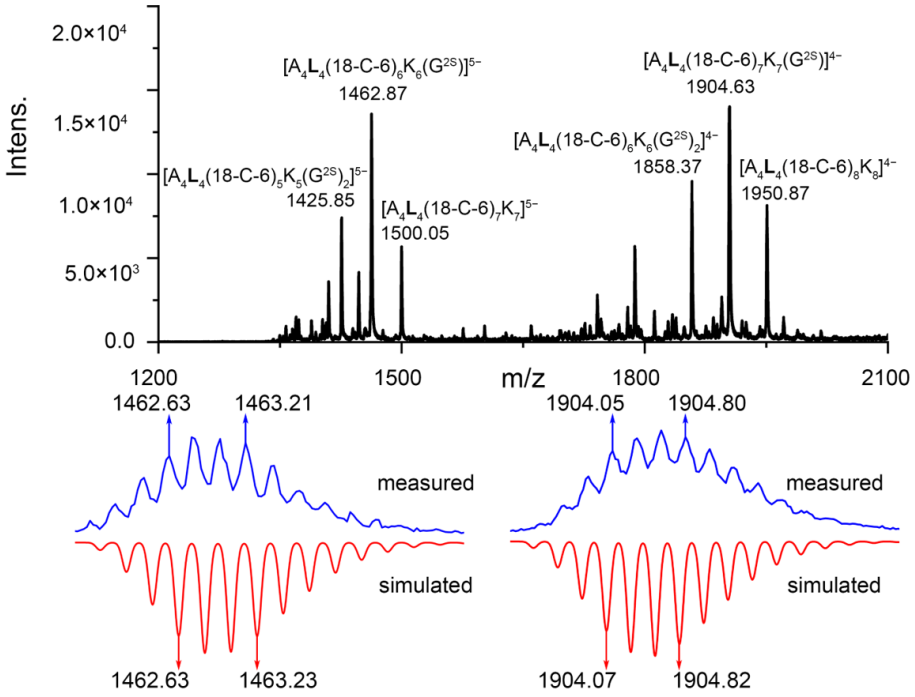

Fig. S36 High-resolution ESI-mass spectrum of **1**⊃G^{2S}.

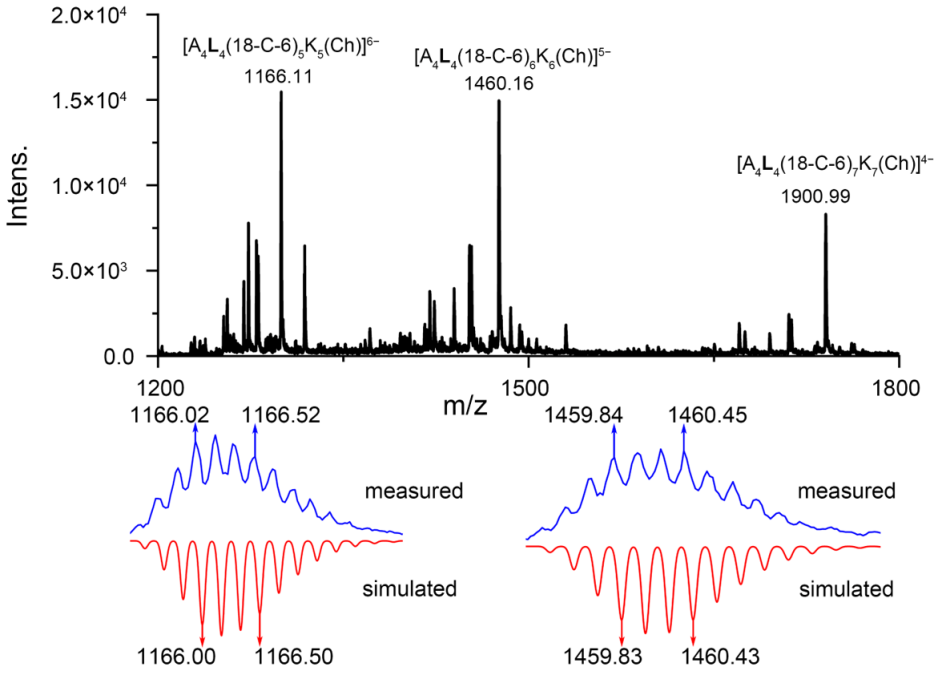

Fig. S37 High-resolution ESI-mass spectrum of **1**⊃Ch^{+}.

S7. Energy calculations

The semi-empirical calculations for ΔΔΔΔ−**1**⊃G^{2R} and ΛΛΛΛ−**1**⊃G^{2R} are optimized by using the PM6 Hamiltonian[7], augmented with empirical dispersion correction (D3)[8]. Based on the optimized geometries, energies were corrected with acetonitrile using the polarizable continuum model (PCM).[9] DFT calculations are also optimized on PM6 optimizations at B3LYP/6-31G level by Gaussian 16 program.[10]

Table S5 The energies of ΔΔΔΔ−**1**⊃G^{2R} and ΛΛΛΛ−**1**⊃G^{2R}.

unit (kcal mol^{-1})		ΔE
PM6	Gas phase	8.64
	Acetonitrile solution	2.53
DFT B3LYP/6-31G	Gas phase	10.56

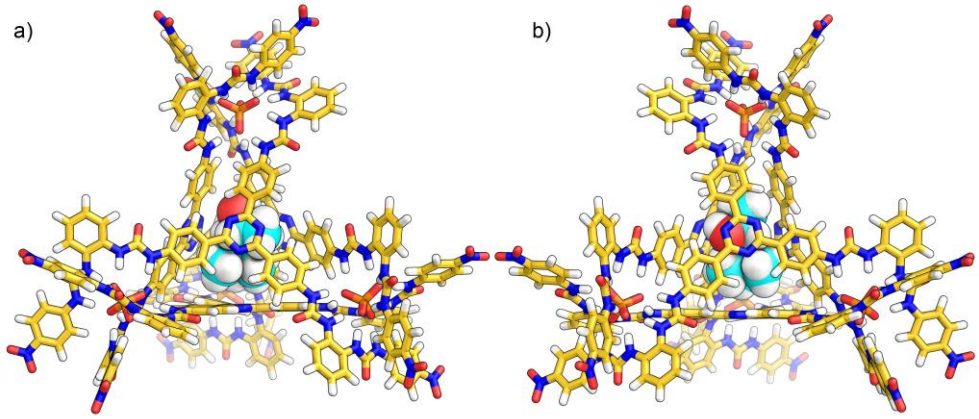

Fig. S38 Optimized structure at PM6 level after corrected with acetonitrile. a) ΔΔΔΔ−**1**⊃G^{2R} and b) ΛΛΛΛ−**1**⊃G^{2R}.

S8. X-ray crystallography

The diffraction data for **1**⊃G^{1R} was collected on a Bruker D8 Venture photon II diffractometer at 150 K with graphite-monochromated Cu-K radiation (λ = 1.54178 Å). The diffraction data for **1**⊃G^{2R} was collected at the BL17B macromolecular crystallography beamline in Shanghai Synchrotron Facility. The collected diffraction data were processed with the KHL3000 software program.[11] An empirical absorption correction using SADABS was applied for the data. The structures were solved by the direct method using the SHELXT program. All non-hydrogen atoms were refined anisotropically by full-matrix least-squares on F^2 by the use of the SHELXL program. Hydrogen atoms bonded to carbon and nitrogen atoms were included in idealized geometric positions with thermal parameters equivalent to 1.2 times those of the atom to which they were attached.

The remaining solvents could not be successfully resolved despite numerous attempts at modeling, and consequently the SQUEEZE function of PLATON was used to account for these highly disordered solvents.

The removed void electron density corresponds to about 0.7 water molecules for **1**⊃G^{1R}**.** In addition, one TBA^+ was refined with restraints. And due to the weak diffractions at higher angles the structure of guest trapped was restrained.

The removed void electron density corresponds to about 19.7 water molecules for **1**⊃G^{2R}**.** In addition, five TBA^+, three $[K([18]crown-6)]^+$ two nitro groups and eight benzene rings were refined with restraints. And due to the weak diffractions at higher angles the structure of guest trapped was restrained.

CCDC 2242757-2242758 contain the supplementary crystallographic data for this paper. These data can be obtained free of charge from The Cambridge Crystallographic Data Centre via www.ccdc.cam.ac.uk/data_request/cif.

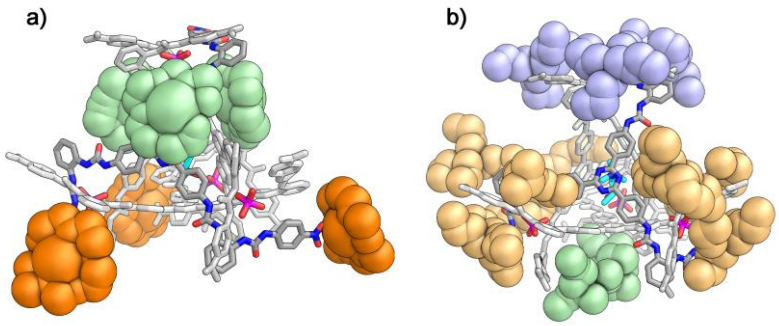

Fig. S39 a) Peripheral [K([18]crown-6)]$^{+}$, b) peripheral TBA^{+} in **1**⊃G^{2R}.

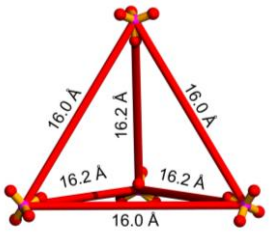

Fig. S40 The $PO_4^{3-}\cdots PO_4^{3-}$ distances in **1**⊃G^{2R}.

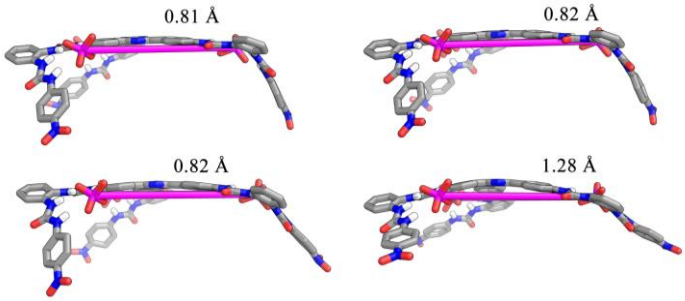

Fig. S41 The distances between the triazine plane and the triangular face of the tetrahedron.

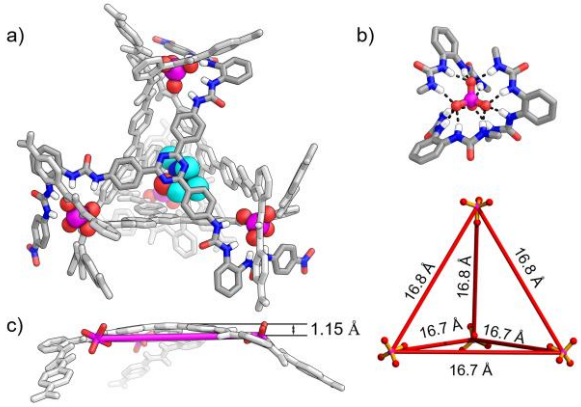

Fig. S42 a) X-ray single-crystal structure of $(TBA)_{11}[(PO_4)_4\mathbf{L}_4\supset G^{1R}]$ (**1**⊃G^{1R}), b) hydrogen bonding between urea groups and PO_4^{3-}, c) the longer distance between the triazine plane and the triangular face of the tetrahedron, d) $PO_4^{3-}\cdots PO_4^{3-}$ distances in **1**⊃G^{1R}.

Table S6 Crystal data of **1**⊃G^{1R}, **1**⊃G^{2R}.

	1⊃G^{1R}	**1**⊃G^{2R}
Empirical formula	$C_{876}H_{816}N_{173}O_{134}P_8$	$C_{735}H_{598}K_7N_{161}O_{172}P_8$
Formula weight	16158.73	14959.17
Crystal System	Trigonal	Monoclinic
Space group	*R*-3c	*C*2/c
a (Å)	39.1474(5)	65.04(3)
b (Å)	39.1474(5)	37.519(16)
c (Å)	111.4756(16)	41.93(3)
α (deg)	90	90
β (deg)	90	121.08(2)
γ (deg)	120	90
V (Å3)	147950(4)	87633(85)
Z	6	4
Dcalc, g/cm3	1.088	1.134
No. of unique data	29003	68161
T (K)	150.01	150
Total no. of data	521084	454525
Crystal size (mm)	0.21 × 0.18 × 0.13	0.25 × 0.20 × 0.18
θ range	2.257 – 66.607	0.732 – 24.110
Completeness to θ	99.7	97.8
Goodness-of-fit on F2	1.068	0.913
R1	0.1115	0.1498
wR2	0.3165	0.3706

*

$$R1 = \sum \| F_O | - | F_C \| / \sum | F_O | \quad \text{for} \quad F_O > 2\sigma(F_O); \quad wR2 = \left(\sum w \left(F_O^2 - F_C^2 \right)^2 / \sum \left(wF_C^2 \right)^2 \right)^{1/2} \quad \text{all reflections} \quad w = 1 / \left[\sigma^2 \left(F_O^2 \right) + (0.2000P)^2 \right]$$

where $P = \left(F_O^2 + 2F_C^2 \right) / 3.$

Table S7 Hydrogen bonds around the PO_4^{3-} ions in **1**⊃G^{1R}.

	D−H···A	d(D−H)	d(H···A)	d(D···A)	∠(DHA)
P1	N5−H5···O1	0.88	1.93	2.787(2)	165
	N21−H21···O1	0.88	1.90	2.753(3)	163
	N22−H22···O1	0.88	1.93	2.790(3)	165
	N16−H16···O2	0.88	1.97	2.788(2)	154
	N17−H17···O2	0.88	1.91	2.770(3)	166
	N23−H23···O2	0.88	1.93	2.798(3)	169
	N3−H3···O3	0.88	1.95	2.803(3)	164
	N4−H4···O3	0.88	1.91	2.777(3)	168
	N18−H18···O3	0.88	1.91	2.749(3)	158
	N2−H2···O4	0.88	2.17	2.923(3)	144
	N15−H15···O4	0.88	2.14	2.9537(16)	153
	N20−H20···O4	0.88	2.24	3.009(3)	146
P2	N10−H10···O5	0.88	2.23	2.9693(18)	141
	N11−H11···O6	0.88	1.87	2.727(2)	166
	N12−H12···O6	0.88	2.02	2.875(3)	164
	N13−H13···O6	0.88	1.98	2.840(2)	167

Table S8 Hydrogen bonds around the PO_4^{3-} ions in **1**⊃G^{2R}.

	D−H···A	d(D−H)	d(H···A)	d(D···A)	∠(DHA)
P1	N7−H7···O1	0.86	1.85	2.694(3)	166
	N41−H41···O1	0.86	1.88	2.692(3)	156
	N42−H42···O1	0.86	1.84	2.682(3)	167
	N43−H43···O2	0.86	1.84	2.662(3)	160
	N69−H69A···O2	0.86	1.85	2.687(3)	164
	N70−H70···O2	0.86	1.86	2.690(3)	163
	N5−H5···O3	0.86	1.80	2.638(3)	164
	N6−H6···O3	0.86	1.83	2.675(3)	169
	N71−H71A···O3	0.86	1.81	2.647(3)	165
	N4−H4···O4	0.86	2.20	2.931(3)	143
	N40−H40···O4	0.86	2.00	2.778(3)	150
	N68−H68A···O4	0.86	2.04	2.804(3)	148
P2	N14−H14···O5	0.86	2.06	2.840(3)	150
	N22−H22···O5	0.86	2.08	2.850(3)	149
	N50−H50···O5	0.86	2.06	2.826(3)	147
	N17−H17···O6	0.86	1.89	2.688(3)	155
	N23−H23···O6	0.86	1.80	2.628(3)	162
	N24−H24···O6	0.86	1.83	2.674(3)	169
	N25−H25···O7	0.86	1.89	2.685(3)	153
	N51−H51···O7	0.86	1.80	2.641(3)	166
	N52−H52···O7	0.86	1.85	2.693(3)	167
	N15−H15···O8	0.86	1.81	2.636(3)	162
	N16−H16···O8	0.86	1.85	2.689(3)	166
	N53−H53···O8	0.86	1.89	2.690(3)	154
P3	N28−H28···O9	0.86	1.86	2.684(3)	160
	N29−H29···O9	0.86	1.82	2.667(3)	167
	N48−H48···O9	0.86	1.89	2.727(3)	165
	N27−H27···O10	0.86	2.03	2.800(3)	149
	N45−H45···O10	0.86	2.13	2.889(3)	147
	N63−H63A···O10	0.86	2.04	2.788(3)	145
	N30−H30···O11	0.86	1.86	2.633(3)	149
	N64−H64···O11	0.86	1.84	2.678(3)	163
	N65−H65···O11	0.86	1.85	2.696(3)	166
	N46−H46···O12	0.86	1.81	2.638(3)	162
	N47−H47···O12	0.86	1.84	2.686(3)	168
	N66−H66···O12	0.86	1.82	2.651(3)	163
P4	N12−H12···O13	0.86	1.85	2.671(3)	159
	N59−H59A···O13	0.86	1.85	2.675(3)	161
	N60−H60A···O13	0.86	1.85	2.694(3)	165
	N10−H10···O14	0.86	1.90	2.698(3)	154
	N11−H11···O14	0.86	1.84	2.686(3)	166
	N35−H35···O14	0.86	1.86	2.705(3)	168
	N9−H9···O15	0.86	2.03	2.804(3)	149
	N32−H32···O15	0.86	2.16	2.910(3)	146
	N58−H58···O15	0.86	2.04	2.790(3)	146
	N33−H33···O16	0.86	1.78	2.611(3)	163
	N34−H34···O16	0.86	1.83	2.674(3)	167
	N61−H61···O16	0.86	1.81	2.643(3)	161

S9. References

1 W. Zhang, D. Yang, J. Zhao, L. Hou, J. L. Sessler, X.-J. Yang and B. Wu, *J. Am. Chem. Soc.*, 2018, **140**, 5248-5256.

2 B. Li, B. Zheng, W. Zhang, D. Zhang, X.-J. Yang and B. Wu, *J. Am. Chem. Soc.*, 2020, **142**, 6304-6311.

3 T. Ishi-i, M. Crego-Calama, P. Timmerman, D. N. Reinhoudt and S. Shinkai, *J. Am. Chem. Soc.*, 2002, **124**, 14631-14641.

4 J.-T. Li, L.-X. Wang, D.-X. Wang, L. Zhao and M.-X. Wang, *J. Org. Chem.*, 2014, **79**, 2178-2188.

5 Y. Wang, H. Fang, W. Zhang, Y. Zhuang, Z. Tian and X. Cao, *Chem. Commun.*, 2017, **53**, 8956-8959.

6 Y. R. Hristova, M. M. J. Smulders, J. K. Clegg, B. Breiner and J. R. Nitschke, *Chem. Sci.*, 2011, **2**, 638-641.

7 J. J. P. Stewart, *J. Mol. Model.*, 2007, **13**, 1173-1213.

8 S. Grimme, J. Antony, S. Ehrlich and H. Krieg, *J. Chem. Phys.*, 2010, **132**, 154104.

9 J. Tomasi, B. Mennucci and R. Cammi, *Chem. Rev.*, 2005, **105**, 2999-3094.

10 M. J. Frisch, G. W. Trucks, H. B. Schlegel, G. E. Scuseria, M. A. Robb, J. R. Cheeseman, G. Scalmani, V. Barone, G. A. Peters-son, H. Nakatsuji, X. Li, M. Caricato, A. V. Marenich, J. Bloino, B. G. Janesko, R. Gomperts, B. Mennucci, H. P. Hratchian, J. V. Ortiz, A. F. Izmaylov, J. L. Sonnenberg, D. Williams-Young, F. Ding, F. Lipparini, F. Egidi, J. Goings, B. Peng, A. Petrone, T. Henderson, D. Ranasinghe, V. G. Zakrzewski, J. Gao, N. Rega, G. Zheng, W. Liang, M. Hada, M. Ehara, K. Toyota, R. Fukuda, J. Hasegawa, M. Ishida, T. Nakajima, Y. Honda, O. Kitao, H. Nakai, T. Vreven, K. Throssell, J. A. Montgomery, Jr., J. E. Peralta, F. Ogliaro, M. J. Bearpark, J. J. Heyd, E. N. Brothers, K. N. Kudin, V. N. Staroverov, T. A. Keith, R. Kobayashi, J. Normand, K. Raghavachari, A. P.

Rendell, J. C. Burant, S. S. Iyengar, J. Tomasi, M. Cossi, J. M. Millam, M. Klene, C. Adamo, R. Cammi, J. W. Ochterski, R. L. Martin, K. Morokuma, O. Farkas, J. B. Foresman, and D. J. Fox, *Gaussian, Inc., Wallingford CT.*, 2016.

11 Z. Otwinowski and W. Minor, *Methods Enzymol.*, 1997, **276**, 307-326.